NUCLEAR SCIENCE AND ENGINEERING: **175**, 124–134 (2013)

# Nondestructive Assay Measurements Using the RPI Lead Slowing-Down Spectrometer

B. Becker and A. Weltz

*Rensselaer Polytechnic Institute*
*Department of Mechanical, Aerospace and Nuclear Engineering*
*110 8th St., Troy, New York 12180-3590*

J. A. Kulisek

*Pacific Northwest National Laboratory*
*Radiation Detection and Nuclear Sciences Group*
*National Security Division, 902 Battelle Boulevard*
*P.O. Box 999, MSIN J4-60, Richland, Washington 99352*

and

J. Thompson, N. Thompson, and Y. Danon*

*Rensselaer Polytechnic Institute*
*Department of Mechanical, Aerospace and Nuclear Engineering*
*110 8th St., Troy, New York 12180-3590*

*Received July 27, 2012*
*Accepted February 4, 2013*

**Abstract**—*The use of a lead slowing-down spectrometer (LSDS) is considered as a possible option for nondestructive assay of fissile material of used nuclear fuel. The primary objective is to quantify fissile isotopes, particularly $^{239}$Pu and $^{235}$U, via a direct measurement distinguishing them through their characteristic fission spectra in the LSDS. In this paper, we present several assay measurements performed at the Rensselaer Polytechnic Institute (RPI) to support ongoing feasibility studies of the method and to provide benchmark experiments for Monte Carlo calculations of the assay system. A fresh uranium oxide fuel rod from the RPI Walthousen Reactor Critical Facility, a $^{239}$Pu-Be source, and several highly enriched $^{235}$U disks were assayed in the LSDS. The characteristic fission spectra were measured with $^{238}$U and $^{232}$Th threshold fission chambers, which are primarily sensitive to fission neutrons with energies above the threshold. Despite the constant neutron and gamma background from the Pu-Be source and the intense interrogation neutron flux, the LSDS system was able to measure the characteristic $^{235}$U and $^{239}$Pu responses. All measurements were compared to Monte Carlo simulations complementing previous modeling-based studies. It is shown that the available simulation tools and models are well suited to simulate the assay. An absolute calibration technique of the LSDS, which is required to perform quantitative measurements of the assayed fissile materials, is presented.*

## I. INTRODUCTION

Lead slowing-down spectrometers (LSDSs) have been researched for nondestructive assay of nuclear fuel pins to analyze their fissile content. In Europe, Interatom designed and the Karlsruhe Nuclear Research Center in Germany successfully operated an LSDS to assay fresh mixed-oxide fuel pins for fabrication control.[1,2] In the United States, the LSDS of Rensselaer Polytechnic Institute (RPI) was used in the past to assay fresh $^{233}$U- and $^{235}$U-enriched fuel pins.[3,4]

*E-mail: danony@rpi.edu

Because of its ability to assay nondestructively, the LSDS is well suited not only for fresh fuel assay but potentially also for spent fuel assay. The characterization of spent fuel is important for nuclear safeguards and for determining the fuel burnup level in view of reprocessing and recycling of used fuel. Being a direct and independent method, the LSDS assay does not necessarily rely on a priori declared information about the fuel, such as burnup or initial enrichment.

In recent years, several studies have been made to assess the potential of the LSDS for spent fuel assay completely based on computer simulations.[5–12] In particular, the ability to assay a full fuel assembly has been investigated by studying the self-shielding effect within an assembly and by exploring different analysis algorithms to determine quantitatively isotopic masses of unknown samples.[10–12] In these previous studies, it was assumed that the LSDS assay system can be precisely modeled using simulation tools like MCNP (Ref. 13) and current nuclear data.[14,15]

To complement the previous modeling-based studies, several benchmark experiments have been carried out in this work. A fresh fuel pin from the RPI Walthousen Reactor Critical Facility (RCF), a $^{239}$Pu-Be source, and several highly enriched $^{235}$U disks were assayed to characterize the signal of the LSDS for these samples and combinations thereof. These measurements were then used to benchmark the capability of performing precise Monte Carlo simulations of the LSDS instrument. The agreement of the simulation of the absolute detector count rate and the shape of the assay response function with the measured signal is shown. An absolute calibration technique of the assay system is presented. This technique is then used to determine the enrichment of the assayed reference fuel pin.

## II. MEASUREMENT SETUP

In this section the RPI LSDS and the measurement setup are presented. The principles of the LSDS are discussed briefly. More information can be found in Refs. 3, 4, 16, and 17.

### *II.A. The RPI LSDS*

The RPI LSDS consists of a pure [99.99% (Ref. 16)] cubic lead pile with side length of 1.8 m and a total weight of 75 tonnes. The cube is covered with a 0.75-mm thickness of cadmium to prevent room return of escaped and thermalized neutrons. The RPI linear accelerator (linac) directs ~50-MeV electrons on an air-cooled tantalum target located in the center of the lead cube (Fig. 1). Neutrons are produced via $(e,\gamma)$ and $(\gamma,n)$ reactions. The energy distribution of the neutrons is given approximately by an evaporation spectrum with peak energy of 0.46 MeV. These neutrons lose energy in successive collisions with the lead isotopes as time progresses. The neutron energy-time correlation is given by[16]

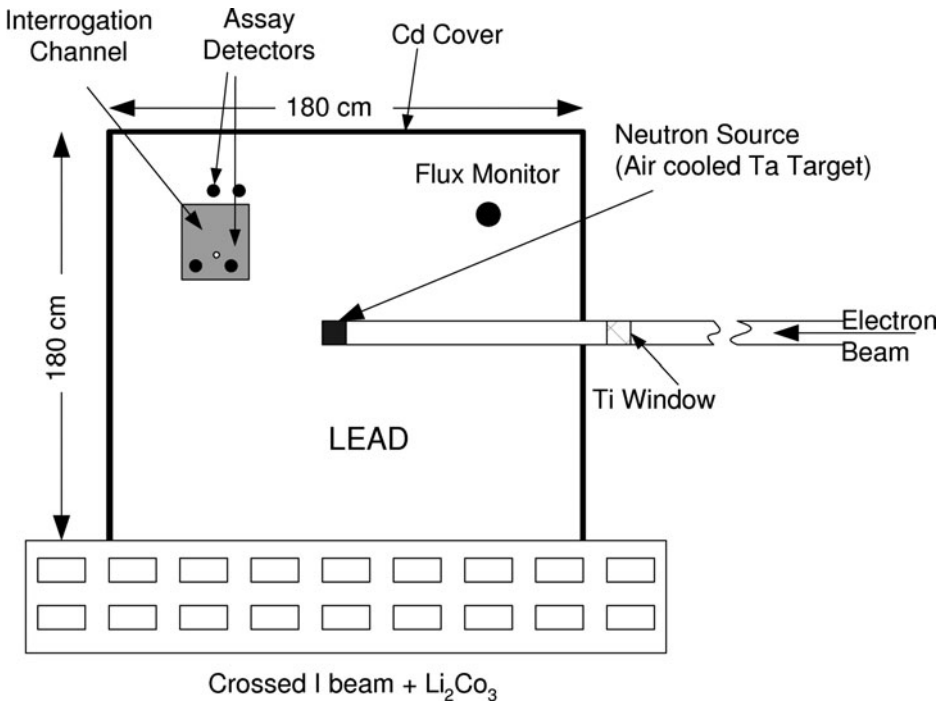


Fig. 1. The RPI LSDS.

$$E = \frac{k}{(t + t_0)^2} \quad , \tag{1}$$

where

$k \approx 165\,000$ eV · $\mu$s$^2$

$t_0 \approx 0.3$ $\mu$s

$E$ = average energy (eV)

$t$ = slowing-down time ($\mu$s).

This direct energy-time correlation is valid shortly after the source pulse until neutrons are completely slowed down. During the slowing-down process, the neutron energy is approximately Gaussian distributed with a time-dependent energy resolution [full-width at half-maximum (FWHM)] of[17]

$$\left[\frac{dE}{E}\right]_{\text{FWHM}} = \left[0.0835 + \frac{0.128}{E} + 3.05 \times 10^{-5} E\right]^{1/2} . \tag{2}$$

It should be noted that the energy resolution is significantly deteriorated with the introduction of impurities of light nuclei such as hydrogen, whether they are in the lead or in the sample itself. The RPI LSDS was therefore built with high-purity lead.[3] The impurities in the lead have been analyzed by mass spectroscopy[18] and are given in Table I.

When a fissile material is introduced into the LSDS, interrogation neutrons cause fission in the sample, creating fission neutrons. Since these fission neutrons have a significantly higher energy than the interrogation neutrons, they can be easily distinguished from the interrogation neutron flux by using a fast neutron detector such as a threshold fission chamber. Each fissile isotope gives a characteristic response as a function of average neutron energy, and thus time [Eq. (1)]. This is mainly due to its specific, energy-dependent fission cross section, which varies significantly with average neutron energy.

TABLE I

Measured Impurities per Gram of Lead in the LSDS*

| Impurity | ($\mu$g/g) | Impurity | ($\mu$g/g) |
|---|---|---|---|
| C | 20.0 ± 0.1 | H | 1.0 ± 0.1 |
| Ag | 1.31 ± 0.01 | B | 0.0 ± 0.1 |
| Cu | 4.52 ± 0.01 | As | 0.04 ± 0.01 |
| Sb | 0.11 ± 0.01 | Ni | 0.15 ± 0.01 |
| Zn | 0.03 ± 0.01 | Cd | 0.01 ± 0.01 |
| Fe | 1.0 ± 0.1 | Sn | 0.03 ± 0.01 |
| Te | 0.19 ± 0.01 | Gd | 0.01 ± 0.01 |
| Sm | 0.01 ± 0.01 | Ti | 2.54 ± 0.01 |
| Bi | 11.53 ± 0.01 | | |

*Reference 18.

### *II.B. Assay Detectors and Flux Monitors*

Two $^{238}$U threshold fission chambers and one $^{232}$Th threshold fission chamber were used to detect the induced fission neutron signal. The assay detectors each contain ~200 mg of $^{238}$U or $^{232}$Th. In the case of the $^{238}$U detectors, highly depleted $^{238}$U is used with a residual $^{235}$U content of 4.1 parts per million (ppm) (Ref. 3). Such high purity is necessary to reduce the contribution of the signal directly caused by the interrogation neutron flux in the detector. The threshold detector response to the interrogation neutron flux is discussed in more detail in Sec. III.A.

The $^{232}$Th detector has a significantly smaller content of fissile impurities [$<25 \times 10^{-9}$ parts of $^{235}$U (Ref. 3)], which increases the signal-to-background ratio. However, since the $^{232}$Th fission cross section is smaller than that of $^{238}$U, the efficiency of the $^{232}$Th assay detector is approximately one-third that of the $^{238}$U detectors. The fission chambers used in this study were manufactured by Westinghouse.[3] Their active length is ~20 cm with a diameter of 2.5 cm. These fission chambers are essentially insensitive to gamma radiation. They are particularly appropriate for fuel assay in an LSDS because they will not be affected by the expected high gamma background caused by the spent fuel and the bremsstrahlung produced by the linac target.

In the presented measurements, the neutron flux is monitored with a small $^{235}$U fission chamber located at the front upper corner of the LSDS (see Fig. 1). This probe detector contains ~1 mg of fissile material. The monitor was used to normalize assay detector signals to the neutron flux in the LSDS.

In a first step, the signal of the fission detectors is amplified with a preamplifier.[a] In a second step, a 100-ns Gaussian shaping amplifier is used. A constant fraction discriminator[b] was employed to discriminate between fission events and background, for example, background caused by alpha particles. The signal amplitude spectrum is used to set the threshold of the discriminator.

Detector signals as functions of time are recorded with a time-of-flight (TOF) clock[c] using a TOF bin width of 409.6 ns. The TOF clock is triggered by a pulse of the linac, which occurs shortly before the electron pulse. The spectra are corrected for the detector dead time and grouped into larger time bins depending on the TOF.

In a last step, the recorded gamma flash is used to determine the time difference between pretrigger and real time of the neutron pulse, and the spectra are shifted to real TOF. Figure 2 shows two examples of recorded

[a] Modified Cremat CR-110.
[b] ORTEC CF 8000.
[c] FAST ComTec MCS6.

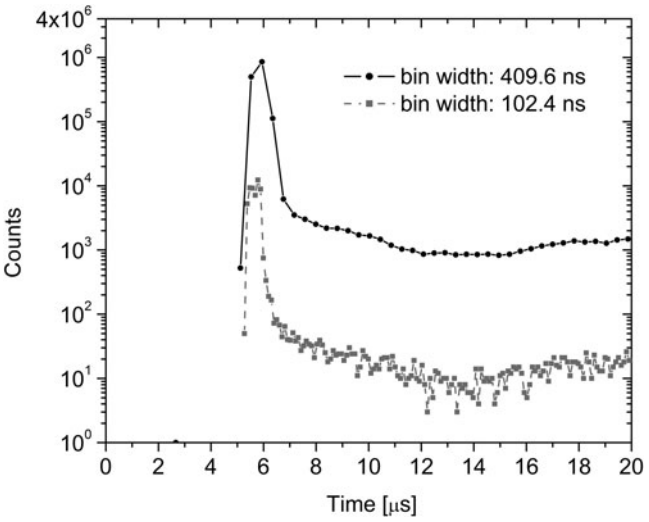


Fig. 2. $^{238}$U assay detector response as a function of time after the pretrigger signal using 409.6- and 102.4-ns time bin widths.

spectra in the first 20 $\mu$s after the pretrigger of the linac using 409.6- and 102.4-ns bin widths. The shown spectra have not been shifted yet, and the gamma flash in both spectra is clearly visible at ~5.5 $\mu$s. With the exception of gamma flash, the used dead-time correction is always <0.5%.

The presented detector, pulse processing, and data acquisition are comparable to what has been considered in some of the design studies (e.g., Refs. 5 and 7) for spent fuel assay.

### *II.C. Assay Specimens: Fresh Fuel Pin, Pu-Be Source, and $^{235}$U Disks*

Three different specimens were assayed in the presented study. A low-enriched $UO_2$ fuel pin of the RCF was used. The fuel pin is 4.8-wt% (4.866 at. %) enriched with 34.8 g $^{235}$U and 689 g $^{238}$U. The active part of the fuel pin has a length of 91.4 cm and a diameter of 1.07 cm. The pin has a 0.05-cm-thick stainless steel cladding. Since the RCF operates at nearly zero-power conditions, the burnup of the fuel pin is negligible, and the pin is therefore considered as fresh fuel.

A Pu-Be source with ~96 g $^{239}$Pu was used as a second assay specimen. The cylindrical Pu-Be source has an outer diameter of 3.58 cm and a length of 8.3 cm. It is assumed that the Pu-Be source was built similarly to as described in Ref. 19. The Pu-Be source serves two purposes: A $^{239}$Pu response function can be measured, and the sensitivity of the assay detectors to a constant neutron and gamma background can be investigated.

Ten highly enriched $^{235}$U disks (93.3%) were used as additional $^{235}$U fissile material. Each disk had an approximate diameter of 1.27 cm and contained between 200 and 300 mg $^{235}$U.

### *II.D. Arrangement in the LSDS*

An interrogation channel (15 × 15 cm) of the LSDS was used to introduce the different assay specimens into the LSDS. One end of the channel was closed permanently with several lead bricks and covered with cadmium and boron plates. The other end was partially covered with one lead brick and a cadmium plate. During the measurement, the fuel pin was supported by fuel grid plates in a fuel assembly box permitting several fuel pin positions. A $^{238}$U assay detector and a $^{232}$Th assay detector were placed directly into the assembly box close to the specimen. An additional $^{238}$U detector was introduced into the lead above the interrogation channel. All detectors were located at mid-depth of the interrogation channel.

### *II.E. Simulation of Detector Responses*

The Monte Carlo code MCNP5 (version 1.51) (Ref. 13) was used to simulate the assay. The entire lead cube, fuel assembly box, and assay specimen were modeled. All neutrons escaping the cube were considered to be lost neglecting the room return of neutrons. Unless otherwise stated, the impurities in the lead were representatively modeled by assuming an $H_2$ content of 1.8 ppm by weight (see Sec. III.B). All cross sections are based on ENDF/B-VII.0 (Ref. 14) with the exception of the cross section of the $^{238}$U content of the detectors, which is based on JEFF3.1 (Ref. 15) (see Sec. III.A). In the model, neutrons are created in the center of the lead cube assuming an isotropic source with the evaporation energy spectrum given by a probability density function of[17]

$$p(E) = Ee^{-E/0.46} \quad , \tag{3}$$

where $E$ is given in mega-electron-volts. Because of the intense neutron scattering, the initial source spectrum impacts the neutron energy and spatial distribution for only a short amount of time after the neutron pulse.[4,17] Several variance reduction methods were applied to decrease the computational time. The lead cube was divided into importance zones increasing the neutron population close to the interrogation channel, i.e., the assay specimen and the detectors. Time weight windows were used to balance the decrease of the neutron population due to absorption and leakage. When simulating only the detector response spectra for the different assay specimen configurations, flux point detectors were used to decrease computational time. However, for absolute count estimation and asymmetrical specimen setup, the flux in the entire detector volume was simulated to take into account geometrical effects due to the length of the assay detectors. A homogeneous detector material was assumed. The bin uncertainty ranged from 0.1% to 2% depending on the assayed sample and the variance reduction method used. A typical computational time for one

configuration was found to be several hours (7 to 10 h) on a 20-CPU 3-GHz i7 Windows cluster.

## III. EXPERIMENTAL RESULTS

During all measurements the linac was operated at 180 Hz and with an electron current and energy range of ~14 to 15 $\mu$A and 40 to 53 MeV, respectively. All measurements were normalized to 14.5-$\mu$A and 46-MeV conditions by using the flux monitor. A typical assay measurement of the fresh fuel pin lasted ~30 to 40 min. Assuming a creation of 0.03 n/e, the typical per-pulse neutron intensity was $\sim 1.5 \times 10^{10}$ n/pulse and the total number of source neutrons was approximately $6.5 \times 10^{15}$.

### *III.A. Threshold Detector Response and Absolute Calibration*

In a first measurement the assay detectors were used without an assay specimen in order to measure the inherent response function of the different detectors. In addition, an absolute normalization of the $^{238}$U detectors can be deduced by using the known $^{238}$U and $^{235}$U content. Figure 3 shows a comparison of the measured response function of the $^{238}$U and $^{232}$Th assay detectors in the fuel assembly box. While the response function of the $^{232}$Th detector shows almost no structure due to the low count rate, the $^{238}$U detector response exhibits a clear structure. A distinct fission peak at ~10 to 20 $\mu$s can be noticed, which is caused by the $^{238}$U subthreshold fission resonances in the 0.4- to 5-keV energy region.[20] The

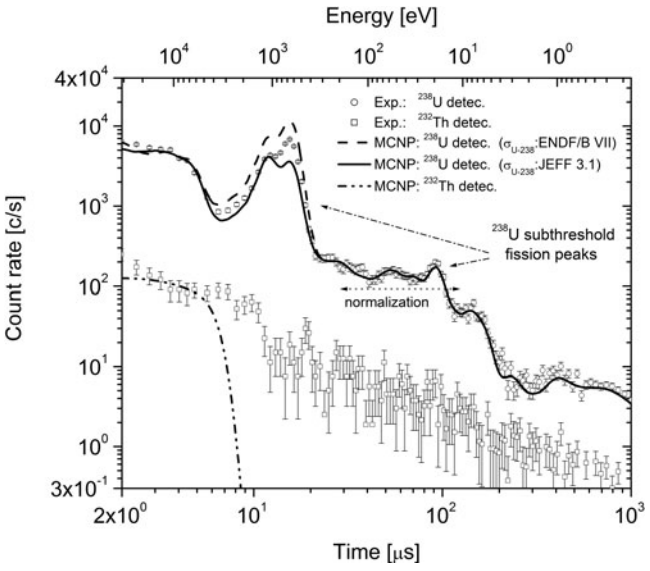


Fig. 3. $^{238}$U and $^{232}$Th assay detector response to interrogation neutrons (experiment: symbols; simulation: lines).

response above 20 $\mu$s is caused by both the $^{238}$U subthreshold fission and the residual $^{235}$U content. Below 10 $\mu$s the $^{238}$U subthreshold fission resonance cluster around 10 keV dominates the response function and the contribution of the residual $^{235}$U content is small.

The response of the $^{232}$Th detector is compared to MCNP calculations using ENDF/B-VII.0. Unfortunately, the fission cross section of the library is zero below the cutoff at ~4 keV.

The response of the $^{238}$U detector is compared to MCNP calculations with either the ENDF/B-VII.0 or the JEFF3.1 cross sections for $^{238}$U. The ENDF/B-VII.0 cross section overpredicts the subthreshold fission peak between 10 and 20 $\mu$s. Using the JEFF3.1 cross section leads to an underprediction of this peak. This difference is caused by a difference of the parameters of the 0.7217- and 1.2113-keV resonances. A similar trend can be noticed by comparing the fission cross sections of these two resonances given in the libraries with the measurement of Block et al.[20] Since the wings of these resonances are slightly better reproduced using JEFF3.1 compared to our measurements, in the following, all cross sections are based on ENDF/B-VII.0 with the exception of the cross section of the $^{238}$U content of the detectors, which is based on JEFF3.1. Besides the differences for these two resonances, there is no noticeable difference between the calculations using ENDF/B-VII.0 or JEFF3.1.

The MCNP calculations of the $^{238}$U detectors were normalized to the experimental data in the 30- to 110-$\mu$s time frame by applying a least-squares method. This time frame was chosen since it includes both a $^{235}$U-dominated region and the $^{238}$U subthreshold peak at 180 $\mu$s. It should be noted that there is also good agreement between simulation and experiment in the $^{238}$U-dominated 2- to 5-$\mu$s time frame as well as in the $^{235}$U-dominated 200- to 1000-$\mu$s time frame. In Secs. III.B through III.G, this normalization in the 30- to 110-$\mu$s range will be used to convert simulated detector counts (given in counts per source particle) to absolute counts, including the detector efficiency and the mass of the active detector material.

In addition to this normalization, the change in strength of the interrogation neutron flux between the calibration and assay measurement has to be taken into account. Such variations in strength can be caused by varying linac conditions, i.e., electron energy and current. In the following, all assay spectra have been divided by the ratio of the flux monitor counts of the assay and calibration measurement.

### *III.B. Fresh Fuel Pin Assay*

Two different fresh fuel pin positions were used: (1) a close position at ~3.4 cm distance to the $^{238}$U assay detectors and (2) a farther position at 8.33 cm distance. The response functions of the $^{238}$U assay detector for the two different fuel pin positions were simulated with MCNP. The simulated response functions

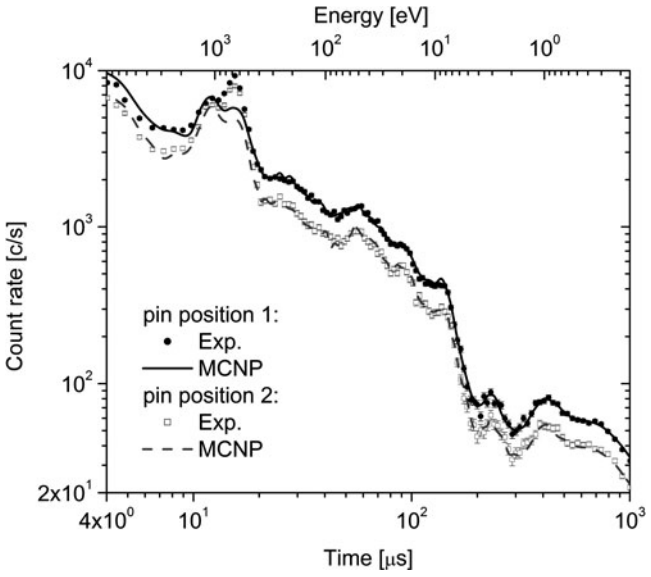


Fig. 4. Fuel pin assay using a $^{238}$U assay detector for two different pin positions (experiment: symbols; simulation: lines).

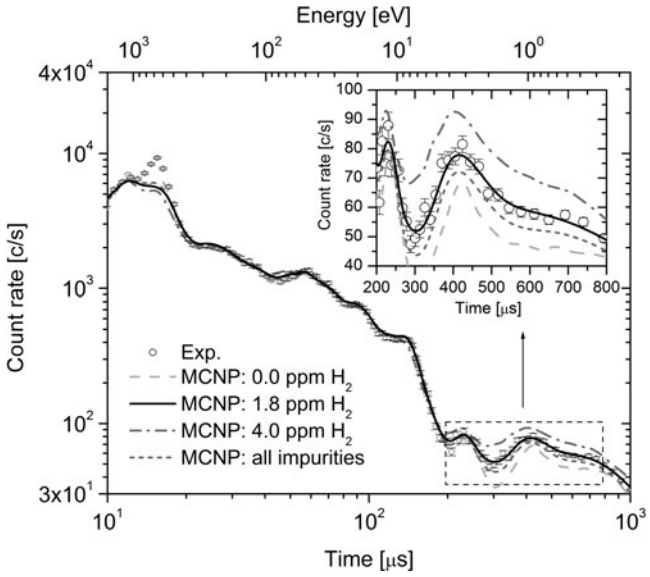


Fig. 5. Impact of $H_2$ impurities in the lead cube on calculation of the single fuel pin assay using a $^{238}$U assay detector (experiment: symbols; simulation: lines).

were converted into absolute count rates by using the normalization region described in Sec. III.A and the flux monitor taking into account the detector efficiency as well as the linac condition. For both positions, the measured and calculated responses are in agreement regarding shape and absolute count rate (Fig. 4).

The resolution of the LSDS is dependent on the amount of light-element impurities in the lead. The higher the impurity level is, the lower the resolution. Several MCNP calculations were made using different levels of $H_2$ contamination and were compared to the assay of the fresh fuel pin. Figure 5 shows the impact of an increasing impurity level in the lead. With increasing hydrogen content, the detector response signal tends to lose structure, which is particularly visible at ~300 $\mu$s. An effective level of 1.8 ppm hydrogen is found to give the best agreement to the experimental response. Using the measured impurities[18] (Table I) in the simulation leads to sharper resonance features of the assay response above 200 $\mu$s. It seems reasonable to assume that the actual hydrogen content in the LSDS might vary from the content measured by mass spectroscopy due to a local increase of the hydrogen concentration in the measurement caused by detector cables and condensation of room humidity. Using an effective hydrogen content to take into account all impurities significantly reduces the run time of the simulation.

To study the sensitivity of absolute count rate calculation to small changes in the enrichment of the fuel pin, several simulations with different enrichments were performed. The ratio of calculation to experiment (C/E) as well as chi squared ($\chi^2$) were calculated in four different time frames all starting at 30 $\mu$s and ranging up to 100, 200, 500, or 1000 $\mu$s (Table II); $\chi^2$ is calculated using

$$\chi^2 = \sum_i \frac{(c_i^{exp} - c_i^{cal})^2}{(\sigma_i^{exp})^2} \quad , \tag{4}$$

where

$c_i^{exp}$ = measured count rate

$c_i^{cal}$ = calculated count rate

$\sigma_i^{exp}$ = uncertainty of the measured count rate.

Assuming a linear relation close to the nominal enrichment (4.866 at. %), a linear regression was used to determine the enrichment of the assayed fresh fuel pin. Enrichments of 4.85, 4.77, 4.78, and 4.81 at. % are deduced for the time frames with upper limits of 100, 200, 500, and 1000 $\mu$s, respectively. The uncertainty of the deduced enrichment due to the counting statistics of the assay and the normalization measurement is calculated to be ~0.1 at. %.

Even though the deduced enrichment is relatively insensitive to the chosen time frame in this specific case of a fresh fuel pin enriched only in $^{235}$U, one has to be aware that this might not be true for a spent fuel pin assay. In the case of a spent fuel pin, the determination of the isotopic amount of fissile material has to include the different specific response functions of different nuclei. Several earlier studies[7,8] investigated different time frames to find an optimal frame to deduce the isotopic composition of a full spent fuel assembly.

TABLE II

C/E and $\chi^2$ of MCNP Simulations of the Fuel Pin Assay Using Different Enrichments and Time Frames*

| $e_{sim.}$ (at. %) | $\frac{e_{sim.}}{e_{nom.}}$ | 30 to 100 $\mu$s | | 30 to 200 $\mu$s | | 30 to 500 $\mu$s | | 30 to 1000 $\mu$s | |
|---|---|---|---|---|---|---|---|---|---|
| | | C/E | $\chi^2$ | C/E | $\chi^2$ | C/E | $\chi^2$ | C/E | $\chi^2$ |
| 4.379 | 0.90 | 0.91 | 386 | 0.93 | 439 | 0.92 | 562 | 0.92 | 646 |
| 4.623 | 0.95 | 0.96 | 194 | 0.97 | 224 | 0.97 | 276 | 0.97 | 295 |
| 4.866 | 1.00 | 1.00 | 68 | 1.02 | 120 | 1.02 | 165 | 1.01 | 171 |
| 5.109 | 1.05 | 1.03 | 168 | 1.05 | 291 | 1.05 | 343 | 1.04 | 365 |
| 5.352 | 1.10 | 1.08 | 402 | 1.08 | 588 | 1.08 | 692 | 1.08 | 782 |
| 5.839 | 1.20 | 1.17 | 1369 | 1.17 | 1870 | 1.17 | 2214 | 1.16 | 2514 |

*$e_{sim.}$: Simulated enrichment; $e_{nom.}$ = 4.866 at. %: nominal enrichment.

### *III.C. Sensitivity of the Assay to Additional Fissile Material*

The accuracy of the fresh fuel pin assay was investigated by performing an assay of the pin and additional small uranium disks. Assays with one, three, five, and ten additional disks were performed. The disks were placed one next to the other on top of the fuel pin. The count rate was integrated from 30 to 110 $\mu$s. Figure 6 shows the increase of the integrated rate as a function of the added mass for the $^{238}$U and $^{232}$Th assay detectors close to the fuel pin and for the $^{238}$U detector in the lead above the interrogation channel.

Because of their close distance to the fuel pin, the response of the detectors in the interrogation channel is dominated by only a section of the fuel pin. The detectors are sensitive to only ~10.6 g out of the 34.8 g $^{235}$U present in the pin. Since the distance between the fuel pin and the detector is significantly larger for the detector above the interrogation channel, it responds to effectively a larger part of the fuel pin. Therefore, the count rate increase is less pronounced when the disks are added to the assay of the fresh fuel pin. With the $^{238}$U in the fuel assembly box it was possible to measure a mass change of ~2.5% using one additional disk.

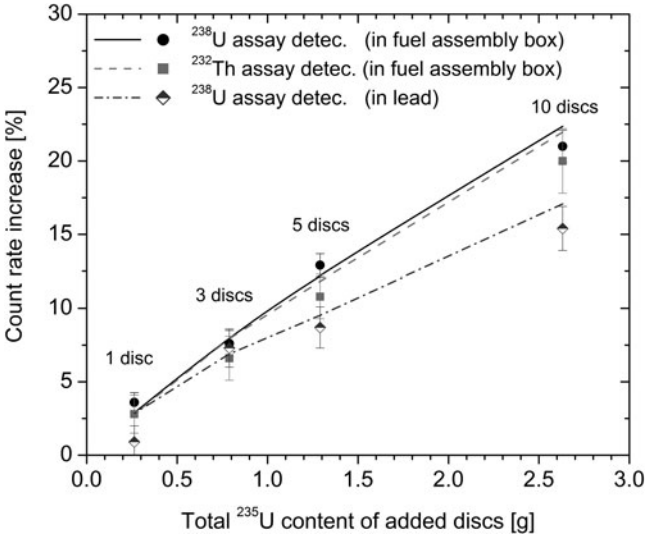


Fig. 6. Assay detector count rate increase due to additional $^{235}$U disks measured with two different $^{238}$U assay detectors and one $^{232}$Th assay detector (experiment: symbols; simulation: lines).

Since the $^{238}$U and $^{232}$Th assay detectors in the interrogation channel are placed at equal distance from the fuel pin, both detectors should measure the same increase of fissile material when disks are added. However, the lower efficiency of the $^{232}$Th detector leads to an increased uncertainty due to counting statistics, which can be noticed in particular for the assay with ten additional disks.

The MCNP simulations of the count rate increase with the additional disks are in good agreement with the measurements for all three detectors with respect to the measurement uncertainty.

The assay presented in this section together with the measurements of the fuel pin at two different positions presented in Sec. III.B illustrates the importance of the detector-sample geometry. Positioning the detector closer to the assay specimen provided better signal statisitics and a more sensitive response to local variations of fissile content. An optimized design of the LSDS was studied by Lee et al.[5,6] using a closely packed bank of detectors and axial translation of the fuel assembly.

### *III.D. Self-Shielding of the Fuel Pin*

Because of neutron absorption in the fuel pin, the neutron flux is depressed toward the center of the fuel pin. This self-shielding effect of the neutron flux depends strongly on the macroscopic cross section of the fuel material and is therefore energy (and time) dependent. The self-shielding within the fuel pin leads to an

additional energy dependence of the fission reaction rate. In a fresh fuel pin, the self-shielding is predominately caused by $^{238}$U absorption resonances and the thermal cross section of $^{235}$U. The response of the fresh fuel pin is therefore different from the response of a $^{235}$U probe chamber, which contains a relatively small amount of $^{235}$U (1 mg). To study the self-shielding effect, the pin response spectrum measured with the $^{238}$U detector was corrected for the background due to the interrogation neutrons (see Sec. III.A). The obtained signal was then compared to the response function of a $^{235}$U probe chamber located at the same position as the fuel pin. The measurement of the probe chamber signal was performed without the fuel pin. Figure 7 shows the ratio of the fresh fuel pin assay signal to the probe chamber signal. The signals were normalized at high energy (between 10 and 30 $\mu$s) where self-shielding effects are assumed to be small. The uncertainty of the experimental data was obtained by propagation of the measurement uncertainties due to counting statistics. MCNP was used to calculate the similar ratio. Figure 7 shows that most of the self-shielding is caused in the resonance region by the lowest $^{238}$U resonances and in the thermal region by the increase of the $^{235}$U cross section. The simulation is in good agreement with the data with the exception of a peak of the experimental data at 30 $\mu$s ($\approx$100 eV). This peak could be caused either by the cladding of the probe chamber or by fissile nuclei other than $^{235}$U in the fuel pin. The shielding effect by the two low $^{238}$U resonances is calculated well.

One has to note that in the case of the assay of a full fuel assembly, self-shielding effects are significantly more complex to calculate than for a single fuel pin as discussed in detail in several publications (see, e.g., Refs. 4, 5, 7, 8, 11, and 12).

### *III.E. Assay of the Pu-Be Neutron Source*

An assay of the Pu-Be source was performed, and the detector signal was compared to the response function of a $^{239}$Pu probe chamber (Fig. 8). The assay detector signal was corrected for the constant neutron background coming from the Pu-Be source, which emits $\sim 10^6$ n/s. Because of the high amount of $^{239}$Pu in the Pu-Be source, the assay detector signal is heavily self-shielded. The strong $^{239}$Pu peak at 100 $\mu$s, for example, is significantly lower than in the case of the probe chamber. In addition, at 200 $\mu$s a dip in the assay detector signal is visible, which is caused by a flux depression of the interrogation neutrons due to resonance absorption of $^{181}$Ta present in the

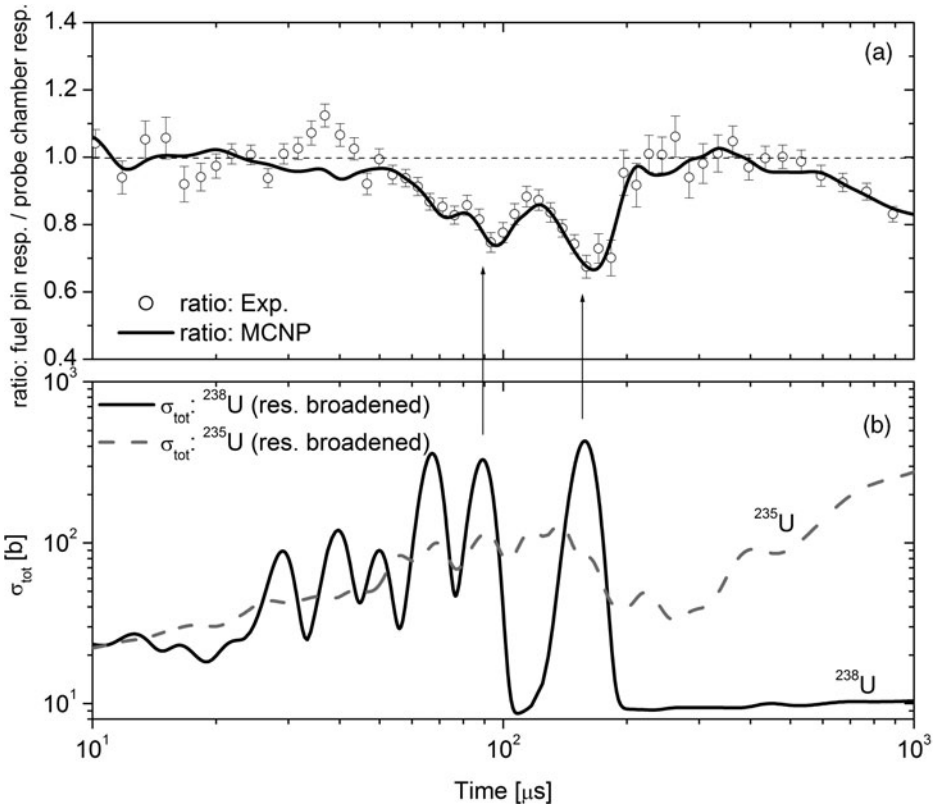


Fig. 7. (a) Self-shielding of the fuel pin measured by comparing the fuel pin assay response with a probe detector response (experiment: symbols; simulation: lines). (b) Resolution-broadened total cross sections of $^{238}$U and $^{235}$U.

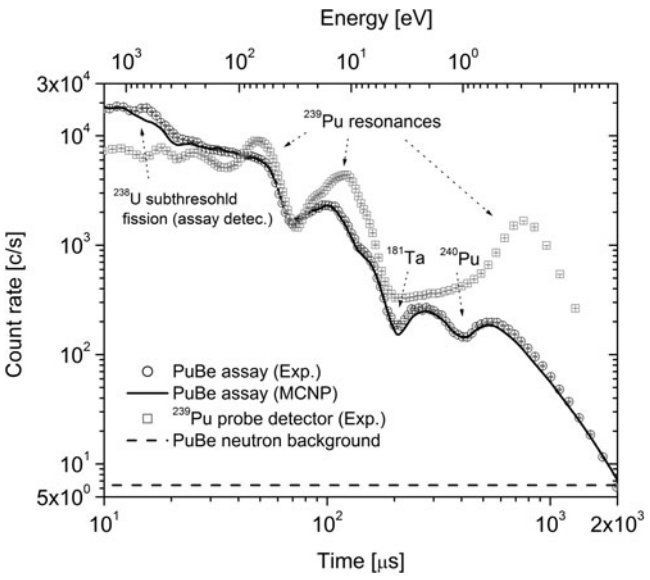


Fig. 8. Comparison of a $^{239}$Pu probe chamber signal (arbitrarily scaled) and an assay detector signal of a Pu-Be source assay (experiment: symbols; simulation: lines).

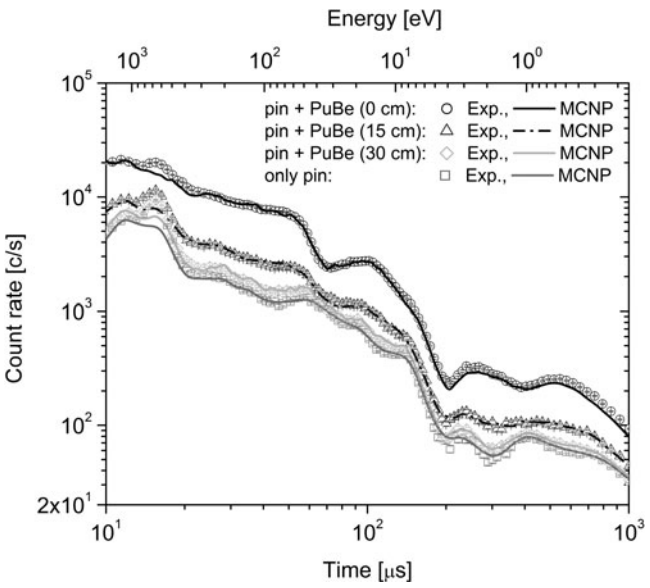


Fig. 9. Assay of a single fuel pin and of a fuel pin and a Pu-Be source at various distances from the center using a $^{238}$U assay detector (experiment: symbols; simulation: lines).

cladding of the Pu-Be source. A similar dip is found at 400 $\mu$s caused by self-shielding due to $^{240}$Pu. Despite these shielding effects, the calculation reproduces the assay detector signal well.

### *III.F. Mixed $^{235}$U and $^{239}$Pu Assay*

A set of mixed $^{235}$U and $^{239}$Pu signals was measured by inserting a Pu-Be source into the LSDS. The contribution of the $^{239}$Pu signal to the detector response was varied by changing the insertion depth of the source, i.e., by changing the distance of the Pu-Be source to the detectors. Figure 9 shows a comparison of the obtained mixed response signals and the response signal of the single fresh fuel pin. Increasing the distance between the source and the center of the LSDS decreases the assay detector response signal due to a decrease of the effective fissile material content. In addition, the shape of the response function changes significantly. The mixed detector signals show characteristics of both the $^{235}$U and $^{239}$Pu response functions. For all cases with the Pu-Be source and the fresh fuel pin, the assay signal can clearly be distinguished from the detector signal caused by only the fuel pin. The constant gamma and neutron background emitted by the Pu-Be source has no significant influence on the assay. Even when the source is centered, i.e., very close to the detectors, the background is easily overcome during the assay.

The combined assay of the fresh fuel pin and the Pu-Be source at the center position was used to perform a linear deconvolution into the base responses of the Pu-Be source and of the fuel pin by minimizing $\chi^2$. The combined assay signal was found to be composed of $0.93 \pm 0.03$ and $0.98 \pm 0.01$ times the fresh fuel pin and Pu-Be source responses, respectively.

Theoretically, the contribution of the $^{239}$Pu to the mixed signal should approximately follow an $\alpha/\bar{R}^2$ behavior, where $\bar{R}$ is the average distance of the source to the assay detectors and $\alpha$ is a normalization constant. Figure 10 shows that this is indeed observed in the measurement. Figure 10a shows the contribution of $^{235}$U and $^{239}$Pu to the mixed signal at various source distances applying a linear deconvolution scheme. Both contributions are given as fractions of the base responses. Figure 10b shows the ratio of the $^{239}$Pu contribution to $\alpha/\bar{R}^2$. $\bar{R}$ was determined by taking into account the dimensions of the detector and the Pu-Be source. $\alpha$ was obtained by normalizing to the $^{239}$Pu contribution when the source is in the center position.

### *III.G. Comparison of the Mixed Assay to the Spent Fuel Assay*

The measured response function of the mixed fresh fuel pin and Pu-Be source assay was compared to a simulation of an assay of a spent fuel pin (Fig. 11). The composition of the spent fuel pin was based on a typical light water reactor pin with an initial enrichment of 4 wt% $^{235}$U, a burnup of 45 GWd/tonne HM, and a subsequent cooling period of 10 years as specified in Ref. 21 as case 13b. The actinide composition used is given in Table III. All main fission products, as described in Ref. 21, were included in the simulation.

The absolute count rate of the spent fuel pin assay is lower compared to the cases of the fresh fuel pin assay

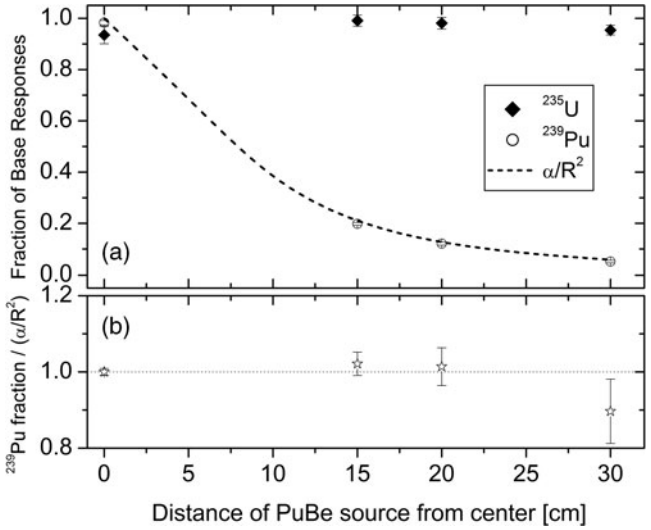


Fig. 10. (a) Deconvolution of the combined fuel pin and Pu-Be source assay into base response functions. (b) Ratio of the $^{239}$Pu contribution and $\alpha/\bar{R}^2$ for $\alpha = 55.3$.

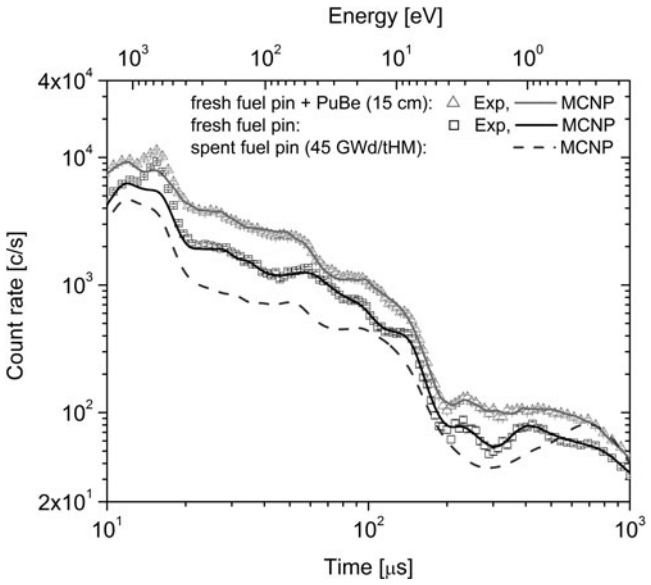


Fig. 11. Comparison of the measured detector signals of an assay of a fresh fuel pin and an assay of a fresh fuel pin and a Pu-Be source with the simulated signal of an assay of a spent fuel pin.

and the mixed assay because of the lower amount of fissile material. The response shapes of the mixed assay and the spent fuel pin assay are to some extent similar in the 40- to 200-$\mu$s time frame. In the spent fuel assay case, the strong $^{239}$Pu fission peak at 700 $\mu$s is observed. As mentioned in Sec. III.E, this peak is completely self-shielded in the Pu-Be source. The inclusion of the 700-$\mu$s peak in the deconvolution of a spent fuel pin assay should in principle improve the quality of the assay. The $^{239}$Pu self-shielding within a spent fuel pin is expected to be significantly smaller than in the presented case of the Pu-Be source, which should improve the distinctness of the contribution of $^{239}$Pu and $^{235}$U fission to the combined signal of a single fuel pin. However, as mentioned in Sec. III.D, one can expect that self-shielding effects are more prominent in the case of a full spent fuel assembly than in the presented mixed assay using a single fuel pin.

TABLE III

Actinide Composition of Simulated Spent Fuel*

| Actinide | (at. %) | Actinide | (at. %) |
|---|---|---|---|
| $^{234}$U | 0.0196 | $^{239}$Pu | 0.6030 |
| $^{235}$U | 0.8613 | $^{240}$Pu | 0.2752 |
| $^{236}$U | 0.5530 | $^{241}$Pu | 0.1295 |
| $^{238}$U | 97.3361 | $^{242}$Pu | 0.0749 |
| $^{237}$Np | 0.0641 | $^{241}$Am | 0.0400 |
| $^{238}$Pu | 0.0271 | $^{243}$Am | 0.0162 |

*Reference 21.

## IV. CONCLUSION

In the present paper, we present assay measurements using the RPI LSDS. Three different samples—a fresh fuel pin, a Pu-Be source, and several highly enriched $^{235}$U disks—were assayed separately and in combination. It was shown that $^{238}$U and $^{232}$Th fast fission chamber assay detectors can overcome the constant neutron and gamma background of the Pu-Be source and the radiation produced at the linac target.

The results were compared to MCNP Monte Carlo calculations of the assay by simulating the entire LSDS. It was demonstrated that the absolute count rate can be correctly calculated when the detector and the LSDS specifications are precisely known, with the exception of a short time frame, dominated by two subthreshold fission resonances of $^{238}$U. The accuracy of the assay and of the calculations was investigated by using different fuel pin positions, determining the enrichment of the fresh fuel pin, and adding the incremental $^{235}$U disks. The self-shielding within the fresh fuel pin could be correctly calculated.

Several assay cases of a fresh fuel pin and a Pu-Be source at different insertion depths were used to mimic, to some extent, the combination of the $^{235}$U and $^{239}$Pu signals in an assay of spent fuel. A linear method was applied to deconvolute the mixed spectra into the base response function of the fresh fuel pin and the Pu-Be source.

The presented measurements and calculations indicated that the available simulation tools and nuclear data

(with the exception of the two identified $^{238}$U subthreshold fission resonances) are well suited to be used in simulation-based LSDS design studies, such as those previously referenced.[5–12] In addition, the presented study supports the ongoing design studies by deploying a detector, pulse-processing, and data acquisition system comparable to what might be used for spent fuel assay.

In a future study, the two mentioned $^{238}$U subthreshold fission cross sections should be corrected in order to use the subthreshold fission peaks as normalization for the detector efficiency determination. It would be worthwhile to repeat some of measurements using a $^{232}$Th detector and a longer measurement time to obtain better statistics with this type of assay detector. In addition, it would be worthwhile to extend the current study by measuring a set of several fresh fuel pins, with and without a Pu-Be source, to include mutual shielding effects of the fuel pins.

## ACKNOWLEDGMENTS

The authors sincerely thank the technical staff at the RPI linac (P. Brand, M. Gray, M. Strock, and A. Kerdoun) for their efforts in operating and maintaining the linac and LSDS and assistance with setting up experiments. This work was supported by U.S. Department of Energy contract DE-AC52-06-NA25396. We also acknowledge the work of the anonymous referees for their valuable comments and suggestions, which improved the original manuscript.

## REFERENCES

1. H. KRINNINGER, S. WIESNER, and C. FABER, "Pulsed Neutron Method for Non-Destructive and Simultaneous Determination of the $^{235}$U and $^{239}$Pu Content of Irradiated and Non-Irradiated Reactor Fuel Elements," *Nucl. Instrum. Methods*, **73**, 13 (1969).

2. H. KRINNINGER, E. RUPPERT, and H. SIEFKES, "Operational Experience with the Automatic Lead-Spectrometer Facility for Nuclear Safeguards," *Nucl. Instrum. Methods*, **117**, 61 (1974).

3. D. S. CRAMER et al., "Lead Spectrometer for Non-Destructive Nuclear Fuel Assay," KAPL-M-7449, Knolls Atomic Power Laboratory (1976).

4. N. M. ABDURRAHMAN et al., "Spent-Fuel Assay Performance and Monte Carlo Analysis of the Rensselaer Slowing-Down-Time Spectrometer," *Nucl. Sci. Eng.*, **115**, 279 (1993).

5. Y.-D. LEE et al., "Design of a Spent-Fuel Assay Device Using a Lead Spectrometer," *Nucl. Sci. Eng.*, **131**, 45 (1999).

6. Y.-D. LEE et al., "Neutron Tomographic Fissile Assay in Spent Fuel Using the Lead Slowing Down Time Spectrometer," *Nucl. Instrum. Methods Phys. Res., Sect. A*, **459**, 365 (2001).

7. L. E. SMITH and N. M. ABDURRAHMAN, "Neutron Spectrometry for the Assay of High Fissile Content Spent Fuel," *Nucl. Technol.*, **140**, 328 (2002).

8. C. ROMANO, Y. DANON, and D. BELLER, "Fuel Assembly Self Shielding of Interrogation Neutrons in a Lead Slowing-Down Spectrometer," *Proc. 6th Int. Topl. Mtg. Nuclear Plant Instrumentation, Control, and Human-Machine Interface Technologies*, Knoxville, Tennessee, March 5–9, 2009, American Nuclear Society (2009).

9. A. GAVRON, L. E. SMITH, and J. J. RESSLER, "Analysis of Spent Fuel Assemblies Using a Lead Slowing Down Spectrometer," *Nucl. Instrum. Methods Phys. Res., Sect. A*, **602**, 581 (2009).

10. L. E. SMITH et al., "Time-Spectral Analysis Algorithms for Lead Slowing-Down Spectroscopy of Spent Fuel," presented at 2009 Institute of Nuclear Materials Management Annual Mtg., Tucson, Arizona, July 12–16, 2009.

11. L. E. SMITH et al., "Time-Spectral Analysis Methods for Spent Fuel Assay Using Lead Slowing-Down Spectroscopy," *IEEE Trans. Nucl. Sci.*, **57**, 2230 (2010).

12. L. E. SMITH et al., "Advancements in Time-Spectra Analysis Methods for Lead Slowing-Down Spectroscopy," presented at 2010 Institute of Nuclear Materials Management Annual Mtg., Baltimore, Maryland, July 11–15, 2010.

13. X-5 MONTE CARLO TEAM, "MCNP—A General Monte Carlo N-Particle Transport Code, Version 5," LA-UR-03-1987, Los Alamos National Laboratory (2003).

14. M. B. CHADWICK et al., "ENDF/B-VII.0: Next Generation Evaluated Nuclear Data Library for Nuclear Science and Technology," *Nucl. Data Sheets*, **107**, 2931 (2006).

15. "The JEFF-3.1 Nuclear Data Library," JEFF Report 21, A. KONING et al., Eds., Organisation for Economic Co-operation and Development (2006).

16. R. E. SLOVACEK et al., "$^{238}$U($n$, $f$) Measurements Below 100 keV," *Nucl. Sci. Eng.*, **62**, 455 (1977).

17. H. M. FISHER, "MCNP Analysis of the LSTDS System to Determine its Feasibility as a Spent Fuel Assay Device," PhD Thesis, Rensselaer Polytechnic Institute (1985).

18. Y.-D. LEE, Korea Atomic Energy Research Institute, Personal Communication (2011).

19. K. L. WAUCHOPE and J. BAIRD, "The Preparation of a Large Plutonium-Beryllium Neutron Source," *J. Nucl. Mater.*, **1**, 191 (1959).

20. R. C. BLOCK et al., "Subthreshold Fission Induced by Neutrons on $^{238}$U," *Phys. Rev. Lett.*, **31**, 247 (1973).

21. A. BARREAU, "Burn-Up Credit Criticality Benchmark, Phase II-D," NEA No. 6227, Organisation for Economic Co-operation and Development (2006).